

Accurate Global Trajectory Alignment using Poles and Road Markings

Haohao Hu¹, Marc Sons² and Christoph Stiller¹

Abstract— Currently, digital maps are indispensable for automated driving. However, due to the low precision and reliability of GNSS particularly in urban areas, fusing trajectories of independent recording sessions and different regions is a challenging task. To bypass the flaws from direct incorporation of GNSS measurements for geo-referencing, the usage of aerial imagery seems promising. Furthermore, more accurate geo-referencing improves the global map accuracy and allows to estimate the sensor calibration error.

In this paper, we present a novel geo-referencing approach to align trajectories to aerial imagery using poles and road markings. To match extracted features from sensor observations to aerial imagery landmarks robustly, a RANSAC-based matching approach is applied in a sliding window. For that, we assume that the trajectories are roughly referenced to the imagery which can be achieved by rough GNSS measurements from a low-cost GNSS receiver. Finally, we align the initial trajectories precisely to the aerial imagery by minimizing a geometric cost function comprising all determined matches. Evaluations performed on data recorded in Karlsruhe, Germany show that our algorithm yields trajectories which are accurately referenced to the used aerial imagery.

I. INTRODUCTION

Using digital maps is substantial for automated driving at the present time. To achieve reliable results from the perception, behaviour generation or planning module in automated vehicles, processed information from current sensor readings is merged and validated with information from digital maps. Actually, maps without any global reference are sufficient to solve the aforementioned tasks since it is not necessary to know exactly where the ego vehicle is in the world but relatively to the map [1]. However, maps generated without exact and absolute global reference measurements usually provide a high local accuracy but worse global consistency. Such maps often show drift and scale errors which reduce the map quality especially when multi-modal and model based filter algorithms are applied for localization. Geo-referencing can be used to correct those errors and improve the global consistency. Furthermore, city-scaled areas are usually mapped from multiple independent recording sessions [2]. To achieve a robust and reliable fusion of all recording sessions into one global frame, an accurate global reference is fundamental. The easiest and most intuitive way to reference driven trajectories globally is to incorporate GNSS measurements into the mapping process. However, due to multipath-, shadowing- and atmospheric drift issues especially in urban areas, only a rough and inconsistent global map accuracy and -reference can be achieved.

¹ Author is with Institute of Measurement and Control Systems, Karlsruhe Institute of Technology, Karlsruhe, Germany. haohao.hu@kit.edu

² Author is with FZI Research Center for Information Technology, Karlsruhe, Germany. sons@fzi.de

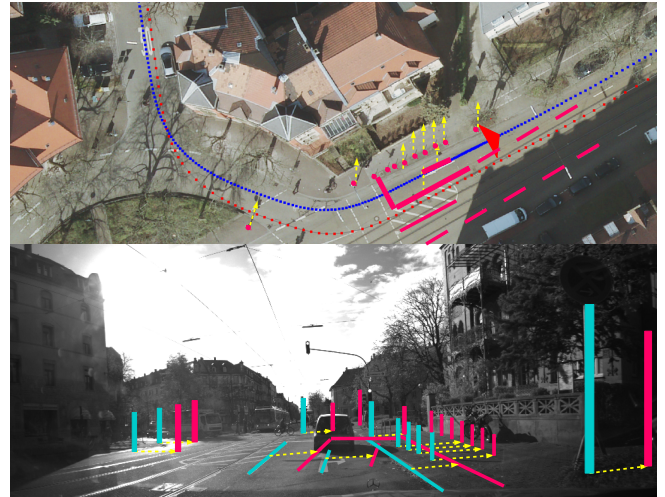


Fig. 1: Depiction of the idea and results of our approach. The top image shows the initial (red) and our post-aligned trajectory (blue). Obviously, the alignment fits well to the road geometry of the underlying aerial imagery. The red triangle shows the view point of the bottom image which shows the displacement (yellow arrows) of pole and road marking features (cyan) which we matched between vehicle sensor readings and aerial imagery landmarks (pink) to align the trajectories accurately. Aerial Imagery: ©Stadt Karlsruhe — Liegenschaftsamt

In this work, we present a novel approach to align trajectories from multiple recording sessions precisely to aerial imagery using pole-like infrastructures and road markings. As input, we assume jointly estimated and roughly geo-referenced trajectories [2]. Since current automated vehicles are usually equipped with cameras and spinning laserscanners, we, furthermore, assume the availability of frequently point cloud and image measurements from each recording session. To improve the global accuracy and geo-referencing, we align the initial trajectories precisely to geo-referenced aerial imagery using feature matches between the vehicle sensor- and the aerial imagery domain. Pole-like structures can be robustly extracted from point clouds and, additionally, distinguished between trees and traffic signs by semantic labelling in the images and successive label transfer into the point cloud domain. Furthermore, road markings can be precisely detected and classified in the images. Since these features are also clearly visible in aerial imagery, provide a good coverage in urban areas and are persistent over long time-periods, we choose them for our approach. To match features robustly between both domains, we propose a novel

sliding window approach. We determine matches in each local window robustly by evaluating randomly selected match hypotheses in a RANSAC scheme [3] using different distance measures. Finally, all matches are treated as constraints in a non-linear least squares (NLS) adjustment problem whose minimization yields the precise global alignment of the initial trajectories.

In summary, we propose a method to postprocess trajectories provided from any multi- or single-session outdoor mapping approach to achieve accurately geo-referenced and globally correct trajectories. By that, we bypass the need of reliable and accurate GNSS measurements. Our main contributions are:

- a selection of geometric features which are on the one hand good observable in the sensor- and aerial imagery domain and on the other hand, establish a good coverage in typical inner-city and sub-urban scenarios.
- a novel RANSAC-based sliding window algorithm to match features robustly between both domains.

II. RELATED WORK

This section reviews state of the art approaches related to this work. Leung et al. [4] presents a monocular vision based particle filter localization in urban environments using aerial imagery as a reference map. Image processing techniques like Canny edge detection and a progressive probabilistic Hough transform are used to create a line feature map from aerial imagery. For localization, line features are detected from ground-based monocular camera image and used as observations. The approach achieves a positioning accuracy of several meters which is a magnitude worse as the accuracy achieved with our approach. Ding et al. [5] analyzes vanishing points to detect 2D corner features from aerial imagery. The same kind of features are also extracted from LiDAR depth maps. A Hough transform and a M-estimator are applied to obtain matches between both domains. Finally, the camera pose is estimated using the obtained 2D corner correspondences. Tournaire et al. [6] proposes an image-based approach for ground-based image to aerial imagery geo-referencing, called "GCO-based geo-referencing (Ground Control Objects)". A Canny edge detector and several basic image processing steps are performed to extract road markings from aerial imagery and ground-based images. Afterwards, an "analysis-synthesis" based matching approach is used for alignment. Instead of using road markings, Bansal et al. [7] uses facades to match street-level images to a database of airborne images. Busch et al. [8] generates a lane-level high definition map of a complex crossing from several static mounted 3D laser scanners. Trajectories provided from dynamic objects passing this crossing are processed within a clustering scheme and a least squares adjustment is finally used to generate a road network automatically. To get the absolute location of the generated map, they extract poles from pointclouds as observations and label them in an aerial image manually as landmarks. An ICP based approach is applied to align the automatically detected poles to the manually measured poles. The approach

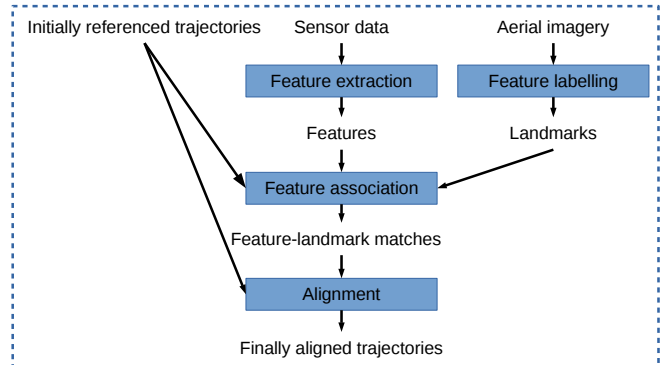


Fig. 2: Overview of the processing pipeline.

achieves a root mean square error of 0.05 m between detected and measured poles. Kümmerle et al. [9] provides a GraphSLAM approach utilizing publicly accessible aerial imagery as prior information to improve the global consistency of maps.

All mentioned approaches align ground-level images to geo-referenced aerial imagery to estimate an absolute ego sensor pose or to stitch all images together. To our best knowledge, there is no existing work which align whole trajectories from multiple independent recording sessions consistently using geo-referenced aerial imagery and multi-modal sensor measurements.

III. ALGORITHM OVERVIEW

In this section, we present the details of our approach which comprises three main processing steps (see Fig. 2). In the first step, features are automatically extracted from the recorded point clouds and images. Additionally, corresponding features (called landmarks in the following) are manually labelled in aerial imagery. Details of this step are described in Sec. III-A. After feature extraction, we robustly match features to landmarks within local areas using our RANSAC-based approach. Sec. III-B describes this matching step in detail. Finally, we solve a NLS problem to achieve the final trajectories. This step is presented in Sec. III-C

A. Feature Extraction

This section describes the extraction and classification process of the used features. We first describe the extraction and classification of pole-like infrastructures. Thereafter, we discuss the recognition of road markings and -boundaries from the recorded images.

For the extraction of pole-like infrastructures from the recorded point clouds, we use a similar approach as in [10]. This approach detects anything which appears like a pole in the point clouds. However, in the aerial imagery only road signs, advertising pillars, traffic lights and boundary posts are discernable. Hence, we classify all detections and keep only the aforementioned types of pole-like infrastructures. For that, we classify the segmented points by label transfer from the image into the point cloud domain. We utilize a modified ResNet38, which is trained using cityscapes-dataset

[11] to obtain pixel-wise semantic labels from the recorded images. Each point of a pole segment is projected into the image using a known sensor calibration and associated with the corresponding pixel label. By max voting over all labels in a segment we obtain the pole label (see Fig. 3).

To detect and classify road markings, we apply the detection and classification approach proposed in [12]. Here, the detected road markings are classified as one of the following classes: arrows, stop-lines, pedestrian crossings, dashed and straight lines with different linewidth. Additionally, boundaries between road and no road are extracted utilizing the semantic labels. These boundaries improve the lateral alignment in areas with less road markings.

B. Feature Matching

As previously mentioned, the extracted features are clearly perceptible in all domains, however, except of rarely occurring arrows, stop-lines and pedestrian crossings, they lack of unique characteristics to match them robustly even with a reasonable prior referencing from GNSS. Fig. 4 shows exemplary aerial imagery landmarks (pink) and, overlaid by the initial trajectories, detected poles (cyan circles) and road markings (cyan line-segments) at a typical crossing. Furthermore, the yellow lines show the displacement vectors of correct matches. Obviously, the feature-landmark displacement is similar within local regions (blue boxes) and varies for different local regions. Therefore, we determine correct matches by estimating a transformation which minimizes the local displacement within a window W . Thereby, the window W is shifted along all mapped areas while keeping an overlap between neighbouring windows.

For matching, poles are represented by their intersection points with the local ground surface. The distance measure for association and optimization is the euclidean distance $d_e(a)$ in this case. Here, a denotes a match between a detected pole feature and a pole landmark. Furthermore, road markings and -boundaries are presented as line segments.

As distance measure for line-segments, we use a modified Hausdorff distance $d_h(a)$ [13]. In this case, a denotes a match between a detected line-segment and a line-segment landmark. Here, we only match line-segments which represents the same class of road marking. For the remaining considerations, we define the generalized feature distance measure

$$d_f(a) = \begin{cases} d_e(a) & \text{if pole} \\ w_h d_h(a) & \text{if line-segment} \end{cases}, \quad (1)$$

where $w_h \in \mathbb{R}$ is a constant factor to weight the line-segment distance relatively to the pole distance.

In the remainder of this section, we describe the RANSAC-based matching which is performed for each W . In each RANSAC iteration, two of all available features in W are randomly selected. The selected features are randomly associated to two different landmarks in the nearby area of the aerial imagery. We assume that the selected areas in both domains are partly comprise the same region of the real world based on the rough initial geo-referencing.



Fig. 3: Exemplary depiction of the label transfer and the max voting whether a pole-like structure is used as feature or not. The green colored bars are accepted as feature since they were labeled as road signs, traffic lights or boundary posts whereas the red colored bar is classified as tree and rejected.

Thereafter, we estimate a single transformation $\Delta_G \in SE(2)$ by minimizing

$$e_f(\Delta_G) = \sum_{i=1}^N d_f(a_i) \quad (2)$$

using the two selected associations ($N = 2$). For optimization, we use the Levenberg-Marquardt (LM) algorithm [14]. In each LM iteration, the features are transformed with the current estimate of Δ_G before evaluating (1). Afterwards, we transform all features in W with the resulting Δ_G and evaluate (2) for all nearest-neighbour matches a_{nn} in W whose distance $d_f(a_{nn})$ is smaller as a pre-setted inlier threshold. This yields the final cost E_f of this iteration. The RANSAC loop terminates until E_f is smaller than a pre-setted threshold E_{limit} or all association combinations are evaluated and no one reached E_{limit} . If $E_f < E_{limit}$, the final matches in W are the inliers of the iteration with the smallest E_f .

Furthermore, we assume that the estimated transformation Δ_G and the transformation $\Delta_{G_{i-1}}$ of the previously estimated and partly overlapping window W_{i-1} are similar. Therefore, we analyze the transformation difference $\Delta_{G_{i-1},G} = \Delta_{G_{i-1}}^{-1} \Delta_G$ in each RANSAC iteration. If the angle $\angle(\Delta_{G_{i-1},G})$ and the absolute translation $\|\text{trans}(\Delta_{G_{i-1},G})\|$ are greater than pre-setted thresholds, we reject the solution of the current iteration. By this, we avoid erroneous transformations caused by e.g. symmetric constellations of feature displacements.

C. Alignment

The final step of our pipeline is the joint alignment of all trajectories to the aerial imagery using the final matches from all windows. The initialization for this optimization is given through the initially referenced trajectories. Here, the poses P from all trajectories are the parameters to be adjusted. Thereby, each $\mathbf{p} \in P \subset SE(3)$ is a 3D-transformation. We minimize

$$e_a(P) = e_f(P) + w_\Delta \sum_{\Delta_{i,j} \in D} \xi(\Delta_{i,j} \mathbf{P}_j^{-1} \mathbf{P}_i) \quad (3)$$

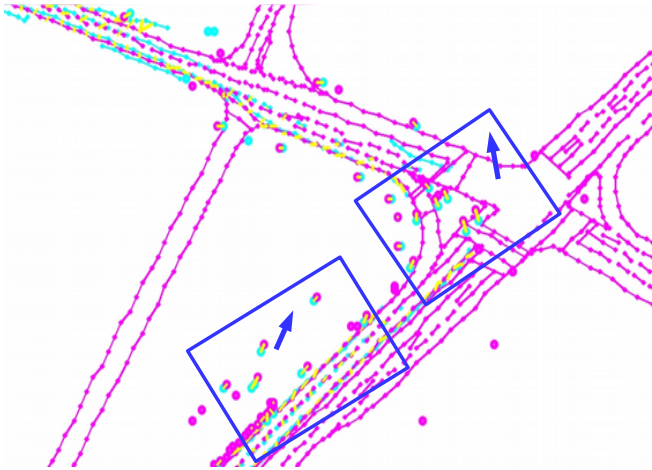


Fig. 4: Schematical depiction of pole and road marking landmarks (pink), pole features (cyan circles), road marking features (cyan line-segments), exemplary matching windows (blue boxes), determined matches (yellow lines) and the computed displacement direction of the windows (blue arrows).

using the LM algorithm. The additional sum in (3) penalizes local distortions between nearby poses $\mathbf{P}_i, \mathbf{P}_j \in P$. Thereby, the $\Delta_{i,j}$ is the original pose difference between \mathbf{P}_i and \mathbf{P}_j from the initialization of P from which we assume that it already exhibits a high local accuracy and smoothness. The topology of the pose difference set D is given from [2]. The $w_\Delta \in \mathbb{R}$ is a constant weighting factor and $\xi : SE(3) \rightarrow \mathbb{R}^6$ depicts a 3D-transformation into a minimal parameterized representation [15]. Similar to the local optimization in the association step, all matched features are transformed based the current estimate of its nearest-neighbour pose in P and the given extrinsic sensor calibration in each LM iteration before evaluating $e_f(P)$ in (3).

IV. EVALUATION

Within this section, we demonstrate the capabilities of the proposed approach. In Sec. IV-A, we briefly describe our experimental vehicle and the evaluation dataset comprising three recording sessions. Afterwards in Sec. IV-B, we introduce two strategies to evaluate the achieved results. Finally, we discuss in Sec. IV-C the trajectory alignment for some typical inner-city scenarios.

A. Experimental Setup

To evaluate our aerial imagery alignment approach, we recorded data with our experimental vehicle *BerthaOne* [16]. The dataset comprises data recorded from four Velodyne VLP16 LiDARs mounted flat on the roof, three BlackFly PGE-50S5M cameras behind the front- and rear windshield and a Ublox C94-M8P GNSS receiver. All sensors are jointly calibrated using the calibration methods proposed in [17] and [18]. The recorded data consists of three partly overlapping passes through sub-urban and inner-city streets in the region of Karlsruhe, Germany (see Fig. 5). All sessions are consistently registered and initially referenced with low-cost GNSS measurements using [2].



Fig. 5: Aerial view of the three jointly aligned and partly overlapping evaluation passes through inner-city and suburban area in Karlsruhe. The green colored bar corresponds to 100m. The entire driven distance is about 19.7km and each recording session is highlighted with a different color (red: 5.5km, blue: 7.5km and yellow 6.7km).

B. Evaluation Method

As for every localization and mapping approach in urban area, where also position estimates from post-processed and RTK-corrected high precision GNSS data lacks in accuracy and robustness, obtaining reliable ground truth data is a unsolved problem. Hence, we evaluate our results with the two following strategies:

- 1) We overlay the initial and the resulting trajectories of our approach to the aerial imagery and analyze carefully every part of the trajectories. This gives a visual hint of the alignment accuracy.
- 2) To evaluate the results more precisely, we project salient environmental structures from an independent HD-map into the recorded images based on the sensor calibration and the finally estimated trajectories with our approach. The HD-map is provided from an external map provider who generated it by a cumbersome semi-automated mapping procedure. By this, we show the alignment accuracy achieved with our approach directly in the recorded images on a pixel-projection level which is highly sensitive to any kind of erroneous alignment.

C. Evaluation Discussion

Fig. 6 shows four exemplary scenarios. The top part of each of the four images shows the initially (red) and our resulting geo-referenced trajectory (blue) overlaid to the aerial imagery. The lower part shows the back projection of the HD-map into the image of one of the front-facing cameras. The triangle depicts the view-point of the camera.

The first two sub-images 6a and 6b show well aligned trajectories. From the overlaid trajectories we see that the

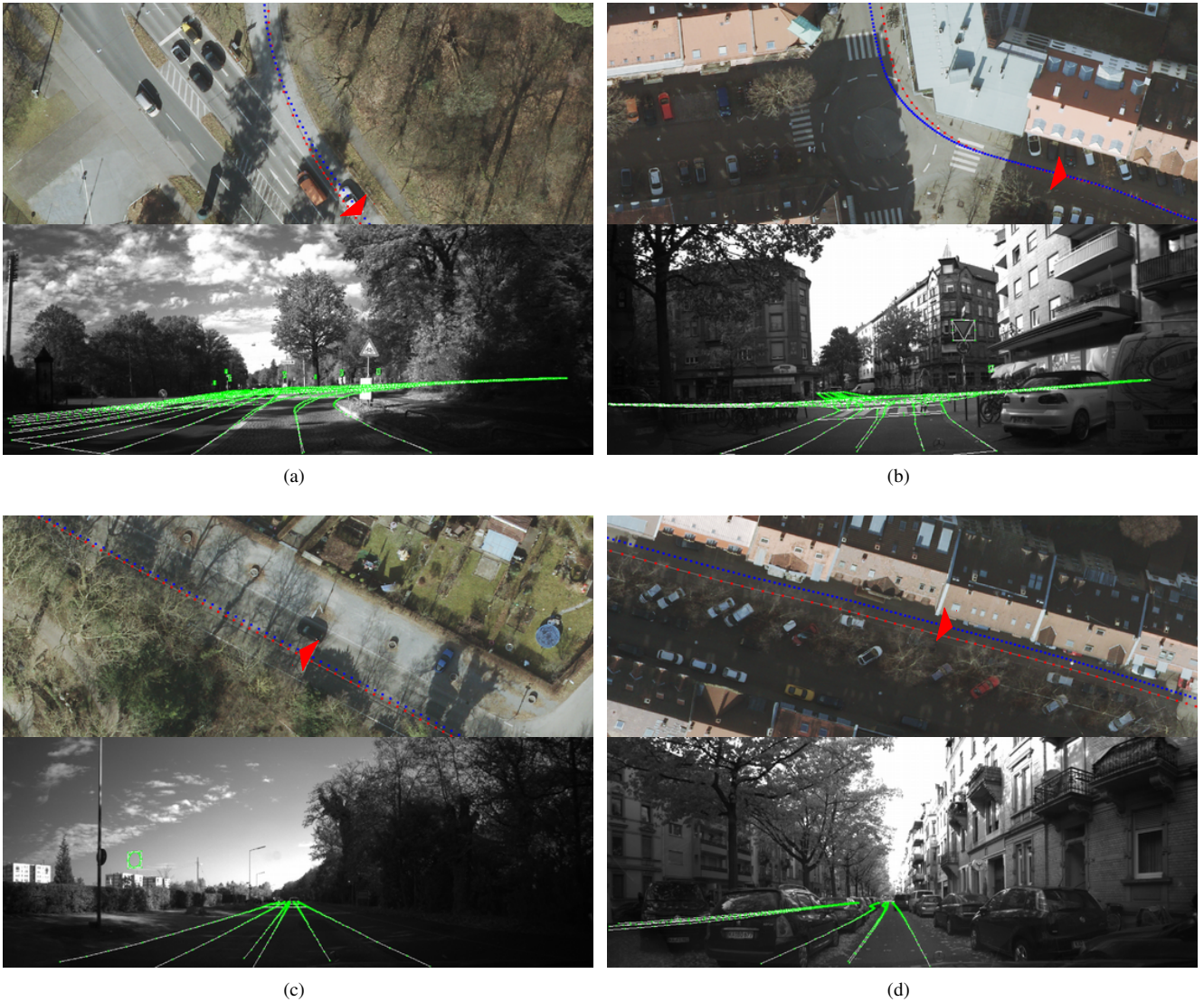


Fig. 6: Evaluation results of exemplary scenarios. The top part of each sub-image shows the initial (red) and the final georeferenced trajectory (blue) overlaid to the aerial imagery. The bottom part shows the back projection of mapped structures of the external HD-map into the recorded images. The red triangle shows the corresponding camera view point. The top two sub-images 6a and 6b show good alignment results whereas the bottom row sub-images 6c and 6d show two of the rarely occurring problem cases.

initially referenced trajectories by GNSS are erroneous since the trajectory is close to the lane boundaries which does not explain our driving behaviour while recording the data since we drove on purpose close to the centerline of the lane. Furthermore, the global orientation and the scale of the initial trajectory appears erroneous. In comparison, our resulting trajectory estimate is well aligned to the centerline which coincides with our driving experience. Furthermore, the lower image of 6a and 6b show the reprojection of salient structures (e.g. lane boundaries and -centerlines, traffic lights, road signs) provided from the independent HD-map into the recorded images using the resulting trajectories. Obviously, the projection of the mapped structures show an accurate placement at the correct positions in the images. Since

the projection into images is particular sensitive to angular errors, these reprojections show the high rotation accuracy. However, also lateral and longitudinal shift errors are clearly visible which occurs rarely if the coverage of features in the area is poor.

The sub-images 6c and 6d show exemplary two of those problem cases. The projection in sub-image 6c shows a sufficient lateral and angular alignment which is visible from the well fitting lane boundaries. However, a longitudinal error is clearly visible by the projection of the road sign in the left part of the image. Here, the poles are not detected in the point clouds due to the high driving velocity and, hence, only the lateral error is observable. Sub-image 6d shows another problem case where road boundaries established by a row of

parked cars are recognized. However, the boundary labels in aerial image fits to the real lane boundaries and, hence, the error minimization leads to a lateral error which is clearly visible.

Table I shows the number of detected and matched features. The road boundary and dashed line 12cm features have by far the highest detection frequency and are almost equally distributed along the passed area which enables an overall well lateral alignment (except of the problem case depicted in sub-image 6d). Poles have also a good coverage but occur more frequently at crossings. More discriminative road markings like arrows, stop lines or zebra lines occurs mainly close to crossings which leads to an excellent alignment at all passed crossings. According to our evaluation, 19.1km of the 19.7km are properly aligned to the aerial imagery. Only at 0.6km, we recognized erroneous alignment as shown in sub-image 6c and 6d. Most of these errors arises from the absence of features and, as a result, a degree of freedom which could not be observed.

session	red	blue	yellow
curb lines	1282 (89.7%)	1627 (92.2%)	1854 (94.4%)
dashed lines 12cm	408 (80.9%)	645 (86.8%)	450 (69.3%)
poles	210 (58.1%)	361 (51.8%)	163 (61.3%)
dashed lines 25cm	46 (82.6%)	89 (84.3%)	115 (69.6%)
lines 12cm	38 (86.8%)	36 (83.3%)	25 (76.0%)
arrow lines	15 (86.7%)	19 (78.9%)	32 (78.1%)
lines 25cm	15 (80.0%)	20 (85.0%)	14 (78.6%)
stop lines	9 (77.8%)	11 (72.7%)	19 (78.9%)
pedestrian road lines	8 (75.0%)	9 (77.8%)	20 (75.0%)
zebra lines	0 (0.0%)	14 (78.6%)	15 (73.3%)
bicycle road lines	3 (100.0%)	9 (66.6%)	6 (83.3%)

TABLE I: Number of detected pole and road marking features. The percentage numbers are the share of successfully matched features.

V. CONCLUSION

Within this work, we presented a novel trajectory georeferencing approach using salient pole- and road marking features which are well observable in the sensor and the aerial imagery domain. We match those features between the two domains robustly by iteratively determining a local displacement error. In our real-world experiments, we showed that our approach achieves accurate results in numerous challenging sub-urban and inner-city scenarios. Our experiments proved the importance of both type of features to achieve a sufficient coverage of measurements and to observe all degrees of freedom. Furthermore, we showed that the alignment using GNSS can not reach this accuracy and robustness due to the lack of reliable measurements.

In summary, our approach allows a reliable joint and globally accurate alignment of trajectories from multiple sessions in areas where GNSS is not reliable which is a fundamental problem of crowd-map based approaches for automated driving.

ACKNOWLEDGMENT

The research leading to these results has received funding from German Federal Ministry of Education and Research

(BMBF) as one part of project UNICARagil. The authors would like to thank BMBF for their support.

REFERENCES

- [1] M. Sons, M. Lauer, C. G. Keller, and C. Stiller, "Mapping and localization using surround view," in *Intelligent Vehicles Symposium (IV), 2017 IEEE*. IEEE, 2017, pp. 1158–1163.
- [2] M. Sons and C. Stiller, "Efficient multi-drive map optimization towards life-long localization using surround view," in *2018 21st International Conference on Intelligent Transportation Systems (ITSC)*, Nov 2018, pp. 2671–2677.
- [3] M. A. Fischler and R. C. Bolles, "Random sample consensus: a paradigm for model fitting with applications to image analysis and automated cartography," *Communications of the ACM*, vol. 24, no. 6, pp. 381–395, 1981.
- [4] K. Y. K. Leung, C. M. Clark, and J. P. Huissoon, "Localization in urban environments by matching ground level video images with an aerial image," in *2008 IEEE International Conference on Robotics and Automation*, May 2008, pp. 551–556.
- [5] M. Ding, K. Lyngbaek, and A. Zakhor, "Automatic registration of aerial imagery with untextured 3d lidar models," in *2008 IEEE Conference on Computer Vision and Pattern Recognition*, June 2008, pp. 1–8.
- [6] O. Tournaire, B. Soheilian, and N. Paparoditis, "Towards a sub-decimeter georeferencing of ground-based mobile mapping systems in urban areas : Matching ground-based and aerial-based imagery using roadmarks," 2006.
- [7] M. Bansal, K. Daniilidis, and H. Sawhney, "Ultra-wide baseline facade matching for geo-localization," 10 2012, pp. 175–186.
- [8] S. Busch, J. Quhel, and C. Brenner, "High definition mapping using lidar traced trajectories," 2018.
- [9] R. Kümmerle, B. Steder, C. Dornhege, A. Kleiner, G. Grisetti, and W. Burgard, "Large scale graph-based slam using aerial images as prior information," *Auton. Robots*, vol. 30, pp. 25–39, 2011.
- [10] M. Sefati, M. Daum, B. Sondermann, K. D. Kreisköther, and A. Kampker, "Improving vehicle localization using semantic and pole-like landmarks," in *2017 IEEE Intelligent Vehicles Symposium (IV)*. IEEE, 2017, pp. 13–19.
- [11] M. Cordts, M. Omran, S. Ramos, T. Rehfeld, M. Enzweiler, R. Benenson, U. Franke, S. Roth, and B. Schiele, "The cityscapes dataset for semantic urban scene understanding," in *Proc. of the IEEE Conference on Computer Vision and Pattern Recognition (CVPR)*, 2016.
- [12] F. Poggenhans, M. Schreiber, and C. Stiller, "A universal approach to detect and classify road surface markings," in *2015 IEEE 18th International Conference on Intelligent Transportation Systems*, Sep. 2015, pp. 1915–1921.
- [13] J. Quehl, H. Hu, . . Ta, E. Rehder, and M. Lauer, "How good is my prediction? finding a similarity measure for trajectory prediction evaluation," in *2017 IEEE 20th International Conference on Intelligent Transportation Systems (ITSC)*, Oct 2017, pp. 1–6.
- [14] S. Agarwal, N. Snavely, S. M. Seitz, and R. Szeliski, "Bundle adjustment in the large," in *European conference on computer vision*. Springer, 2010, pp. 29–42.
- [15] M. Sons, H. Lategahn, C. G. Keller, and C. Stiller, "Multi trajectory pose adjustment for life-long mapping," in *Intelligent Vehicles Symposium (IV), 2015 IEEE*. IEEE, 2015, pp. 901–906.
- [16] Ö. Ş. Taş, N. O. Salscheider, F. Poggenhans, S. Wirges, C. Bandera, M. R. Zofka, T. Strauss, J. M. Zöllner, and C. Stiller, "Making bertha cooperate—team annieways entry to the 2016 grand cooperative driving challenge," *IEEE Trans. Intell. Transp. Syst.*, vol. 19, no. 4, pp. 1262–1276, 2018.
- [17] T. Strauß, J. Ziegler, and J. Beck, "Calibrating multiple cameras with non-overlapping views using coded checkerboard targets," in *Proc. IEEE Intell. Trans. Syst. Conf.*, 2014, pp. 2623–2628.
- [18] J. Kümmerle, T. Kühner, and M. Lauer, "Automatic calibration of multiple cameras and depth sensors with a spherical target," *IEEE/RSJ International Conference Intelligent Robots and Systems (IROS)*, 2018, forthcoming.